Comparative characterization of FDM structures with electrically-conductive sensing elements under static, dynamic and thermal loads

scientific reports

Check for updates

OPEN

Comparative characterization of FDM structures with electrically-conductive sensing elements under static, dynamic and thermal loads

Ferdinando Ursi & Giorgio De Pasquale✉

Fused filament fabrication (FFF), or fused deposition modeling (FDM), is one of the most widely accessible additive manufacturing (AM) processes. Recent advancements in this technology have expanded its material portfolio to include conductive composites with electromechanical properties, enabling new applications. The thermal melting of the filament, required for material extrusion, introduces variability in the final component properties, which are difficult to predict due to the influence of several process-related parameters. In particular, for applications where mechanical and electrical properties are critical, it is essential to optimize the process to control both the mechanical performance and electrical conductivity of the material in static and dynamic conditions. Post-process thermal treatments can significantly alter these electromechanical transduction properties. In this study, we investigate the static, dynamic, and thermal behavior of two composite filaments. The microstructure of the feedstock materials was analyzed using scanning electron microscopy (SEM) to establish a correlation between material composition and component behavior. The results demonstrate that the inclusion of specific fillers, such as black carbon, enhances electrical resistance and improves electromechanical stability under static and dynamic conditions. In contrast, graphene additives increase electromechanical sensitivity but result in a degradation of electrical properties during thermal treatment.

Keywords Conductive filament, FDM, FFF, Additive manufacturing, Sensors, IoT

Fused filament fabrication (FFF), originally called fused deposition modelling (FDM) gained widespread popularity among additive manufacturing (AM) processes due to its accessibility and versatility. In this process, a thermoplastic filament is heated up to the melting point and extruded through a nozzle to build, layer by layer, the three-dimensional object. The main advantages of FDM are the ability to produce complex geometries impossible to achieve with subtractive processes and the availability of machines relatively affordable, easy to use and with reduced production costs compared to other AM processes.

Materials commonly used in FDM are polylactic acid (PLA), acrylonitrile butadiene styrene (ABS), and polyethylene terephthalate glycol (PETG), each offering different mechanical properties and suitability for various applications. PLA is biodegradable and relatively easy to print, ABS is more durable and heat-resistant, making it ideal for functional parts and end-use products, PETG combines the ease of printing of PLA with the strength of ABS, offering a balance of flexibility and durability[1,2].

The layer-by-layer building strategy results in anisotropic properties, meaning the strength of the printed object varies depending on the load direction. Post-processing techniques such as sanding, acetone smoothing, or painting can improve the surface finish and mechanical properties of the printed parts. Despite some limitations, such as slower production speed and lower resolution compared to other AM methods like stereolithography (SLA) and selective laser sintering (SLS), FDM achieved a consolidated level in several industrial sectors involving fast prototyping and small-medium scale production based on cost-effectiveness and ease of use[1,3]. Among these sectors, there are automotive, aerospace, and healthcare. Moreover, the beneficial environmental footprint of FDM materials is an area of active research, because this process can operate on sustainable, recyclable and low-impact options. The advancement of technology is opening to new needing and challenges, then improving print quality, speed, and material properties are being addressed, paving the way for future innovations[4].

Smart Structures and Systems Lab, Politecnico Di Torino, Corso Duca Degli Abruzzi 24, 10129 Torino, Italy. ✉email: giorgio.depasquale@polito.it

The advancement of the FDM process also lead to the integration of new filler materials in the process resulting in polymer composites. Conductive polymer composite (CPC)[5] is a class of material in which the filler materials exhibit electrical conductive properties[6]. Filler materials employed in CPC are mainly classified as metal[7] or carbon-based[8]. Anyway, due to problems related to abrasion and clogging affecting the metal-based, carbon-based CPC are the most recommended when aiming to the production of smart and functionalized components[6].

For example, long fiber filaments are involved in the FDM process as reinforcement material in the so called CFR-FDM (composite fiber reinforcement—FDM) process[9]. When using conductive materials such as long carbon fibers, in addition to improved mechanical properties, the final components will also exhibit enhanced electrical properties. However, long fibers suffer damages during the deposition process itself due to the inherent stresses and mechanical forces involved[10]. This presents a significant challenge in the use of advanced composite materials for 3D printing, necessitating appropriate printing techniques and parameters to minimize such issues.

However, nanomaterials are the most widespread fillers employed to provide the feedstock with electrically conductive properties. Among these, black carbon (CB), carbon nanotubes (CNTs), and graphene particles (GP) are the most promising ones[11,12].

The physical phenomenon that allows the electrical conduction through the nanoparticles composite feedstoks is the percolation theory that describes the electrical conduction in the macroscale as result of conduction mechanisms between filler particles. The percolation threshold is the minimum amount of conductive filler to introduce in the polymer matrix to make it able to exhibit conductive properties[12,13]. As reported by Pejak Simunec et al.[14] the conduction is due to electron tunnelling that consists of electrons "jump" from one filler to the next one across distances through the polymer matrix and/or direct contact of conductive fillers, meaning that electrons transfer happens via conductive filler pathway.

However, other recent studies proved that CPCs can find large application in the manufacturing of smart structures. Several studies demonstrated that such materials are strain-sensitive, thus suitable as strain or pressure sensors[15–18], while others studies highlighted temperature sensitivity and thus potential application as thermometers[19,20]. Maurizi et al. have proposed the application of sensors manufactured via FDM for the dynamic measurements[21] while other studies have investigated the application of these composites in the manufacturing of electrochemical sensors[22,23].

The combination of AM processes and conductive materials has already demonstrated its potential for producing functional, end-use devices. For example, Hook et al. developed a frequency selective surface (FSS) using a conductive material printed via FDM[24], Podsiadły et al. demonstrated the feasibility of manufacturing human interface device (HID)[25] and Jayanth et al. confirmed the suitability of ABS-BC composites for electromagnetic shielding applications[26]. Flowers et al. proposed 3D printed inductors[27], while Hampel et al. manufactured a capacitor with a commercial electrically conductive filament and developed a model of the electrical resistance of 3D printed structures manufactured with FDM[28]. As the FDM process is sensitive to the printing parameters, the use of functional materials exacerbates this criticality as reported by different studies[29–31]. Other cons highlighted by Yu et al. include the shift of the electrical properties when cyclical quasi-statics loads are applied[32]. Several researchers have explored the use of customized filaments to enhance electrical performance. However, this approach makes it more challenging to replicate their experiments and demands greater resources to initiate the process. In a recent study, Aloqalaa reported the current status about the commercially available filament identifying up to twelve different electrically conductive filaments[34].

Many of the aforementioned studies highlight the dependence of the electrical conductivity of CPCs on a single factor (e.g., mechanical stress or temperature) or propose end-use applications while neglecting aspects related to real environmental conditions, making them applicable only under specific circumstances. In contrast to existing studies, the present work adopts a targeted approach to assess the feasibility of smart components equipped with embedded strain sensors. As reported in the literature, temperature is an environmental factor that can influence the performance of strain gauges, along with vibrations[33].

The innovative contribution of the present study consists in a comparative analysis of two commercial CPC for sensing applications. The proposed investigation involves the static and dynamic characterization of the electro-mechanical and electro-thermal behavior of two CPCs, followed by a Scanning Electron Microscopy (SEM) analysis of the tested materials. Similar experimental approaches have been previously applied by the authors in earlier studies[35–39]. Finally, conclusions and remarks are provided regarding the observed behavior of the two materials, evaluating their potential for use in the manufacturing of smart components.

Description of samples

This section describes the samples design, the manufacturing parameters setup and the embedding of electrodes. The samples are specifically fabricated for three test typologies: tensile tests, thermal tests and dynamic tests. All the samples are composed of a base material, with electrically insulating properties, and of a conductive material that is deposited in shape of wires or meander. In total, 18 samples for tensile tests, 6 samples for thermal tests and 2 samples for dynamic tests were fabricated.

Samples geometry

For the tensile and thermal tests, the same sample shape is employed, to use the same printing path and reduce the variability of the process. The geometry of the base material is in agreement with the tensile test standard shape ASTM D638-22 Type V[40], referred to experimental characterization of polymers. Shape and nominal dimensions used for the samples fabrication, through CAD and STL file formats, are reported in Fig. 1a.

The conductive material is deposited on the top surface of the sample with a wire shape in variable widths of 0.4, 0.8, and 1.6 mm. The width of each extruded filament is 0.4 mm, than the three conductive wire variants are obtained with one, two and four parallel depositions respectively. The thickness of each layer is imposed at

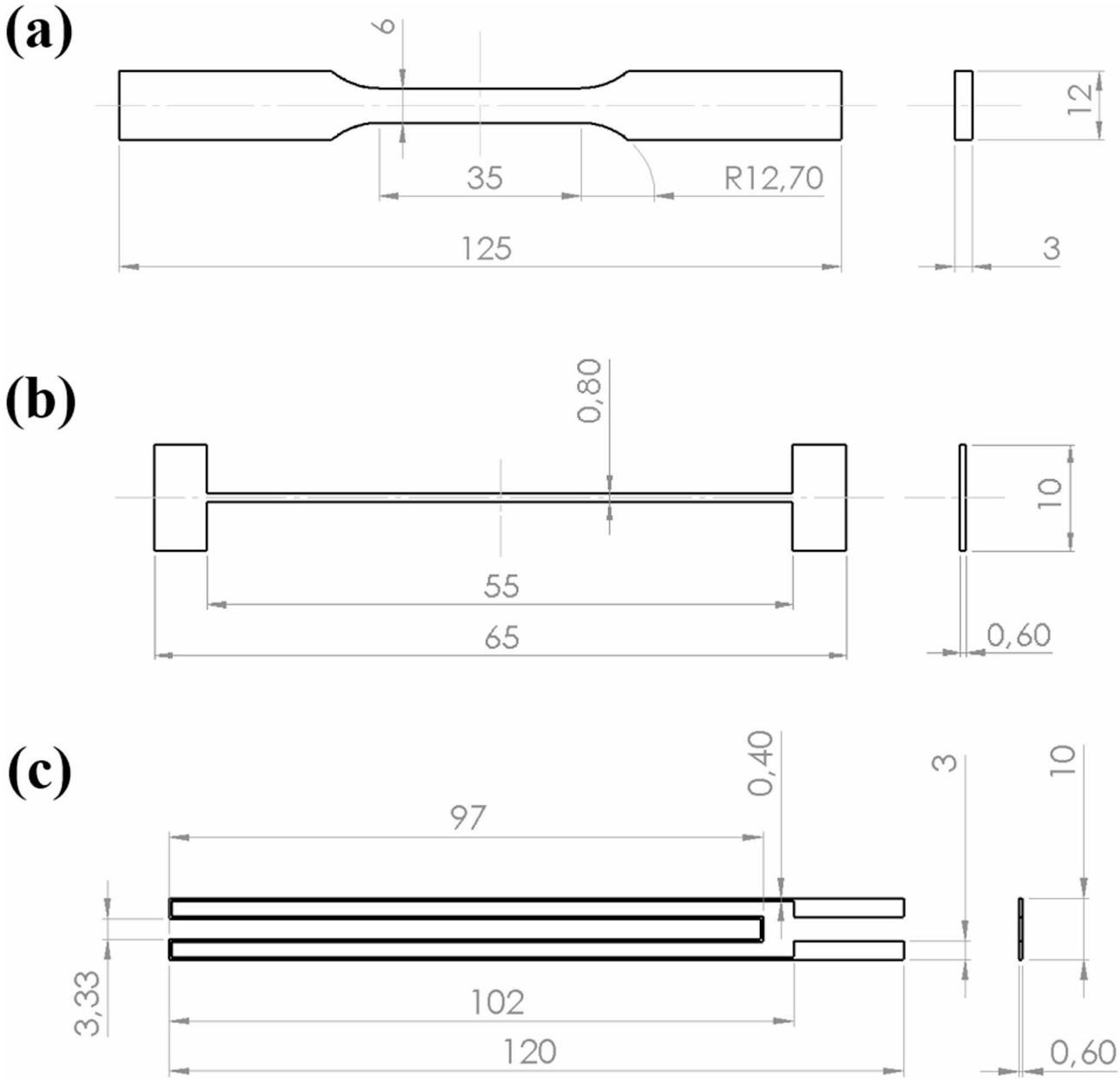

Fig. 1. Specimen shape and dimensions in agreement with ASTM D638-22 Type V for polymers tensile test (**a**), conductive deposited filament (0.8 mm width) and connection pads (**b**), conductive meander for dynamic tests samples (**c**).

0.2 mm for both insulating and conductive materials. At the ends of the conductive path, two connection pads are also fabricated to allow the fastening of copper electrodes used for measurements in the experimental setup. The shape of one conductive stripe (0.8 mm) is represented in Fig. 1b as an example.

The samples for dynamic tests consist in a beam with dimensions $125 \times 12 \times 3$ mm^3, with a conductive meander printed on the top surface with geometry and dimensions reported in Fig. 1c. This regular shape is used to simplify the modelling of the beam response. The conductive meander amplifies the electric output signal and reduces the noise respect to the single wire, which allows dynamic measurements. Similarly to the previous conductors, connection pads are fabricated at the ends of the meander to fasten the electrodes.

Materials and fabrication process

The samples are fabricated with the UltiMaker S5 multi-material system, equipped with the dual-extruder device. The material used for the structural part of the samples is the PLA Pro1-white, provided by BASF. The matrix polymer selected for the study is the thermoplastic polyurethane (TPU), a polymer with considerable elongation at break, able to accommodate the structure during the deformation without occurring in fracture.

The two CPC considered for the experimental characterization are "Fili", provided by AIMPLAS Technological Institute of Plastics, and the other one is called "Filaflex Conductive", provided by RECREUS.

According to the information provided by the manufacturers, the "Fili" material, using graphite particles as conductive filler, has 27.44 Ω·cm electrical resistivity. The "Filaflex Conductive" material, including carbon black conductive filler, has 3.9 Ω·cm resistivity[41]. The filler concentration as volume percentage is defined by the producer by considering several constraints, as the shape and typology of the same filler, and the expected physical properties of the filament. In particular, higher concentrations led to higher conductivity but also higher viscosity and brittleness, causing extrusion and homogeneity issues of the filament.

The printing of the samples is preceded by the optimization of the printing parameters. Due to the presence of fillers, the filaments viscosity and their propensity to the extrusion are sensitively different from their filler-free versions. For this reason, compared to the standard parameters recommended in the material datasheet, further improvements of the printability are achieved by reducing the printing speed and by increasing the flow rate. The Table 1 summarizes the most relevant parameter resulting from the optimization of the printing process.

The fabrication process is driven by the slicer software UltiMaker Cura Enterprise (v. 5.6.0), that is used to perform the optimization process and to manage the printing. The selected layer height is 0.2 mm to achieve good dimensional resolution and reasonable printing time. Through the multi-material functions of the software, it is possible to assign different materials to specific geometries imported with separate STL files. By using the merging functions, the dual-extrusion process is optimized to make a continuous transition at the borders. Moreover, through the programming of the G-CODE embedded into the slicer software, it is possible to interrupt the deposition process at a specific layer for a given time and restart the process after the manual operations on samples are completed.

Electrodes coupling

The physical connection between the conductive material and the instrumentation must provide good adhesion and low concentrated resistance to prevent measurement errors and achieve stable electric output. The electrical resistance of the deposited filaments is measured in the following tests. In other experiments[11,19,21], this connection is obtained by means of conductive inks applied between the conductive material under investigation and external electrodes. However, the conductive ink shows generally low mechanical reliability and properties variation over time. Then, in this study, two copper plates are embedded into the sample during the growth process and then used as electrodes for connecting the instrumentation. The growth process is interrupted after the deposition of the first conductive layer on the top surface of the base material. At this point, the copper plates are positioned on the corresponding contacting pads at the ends of the conductor. By using a jig and tape, the copper plates are secured in that position and the printing process is completed with two additional layers of conductive material. The jig and tape protect the copper plates against undesired movements induced, for example, by the nozzle motion. The sample with embedded electrode is represented in the drawing of Fig. 2a and the fabrication steps are reported in Fig. 2b. Before the embedding process, the edges of the copper plates are shaped in a saw-teeth profile and folded. This shape of the plate edges provides a stronger anchoring with the polymer and an interface more stable mechanically.

After the samples fabrication, the electro-mechanical properties of the electrodes connection are validated. The mechanical strength is evaluated manually by ensuring that relative movement between the copper plate and the polymer is present. The electric resistance of each connection is measured, obtaining for all the samples values below 0.1 Ω.

Experimental tests

This section describes the three tests setup for tensile, dynamic and thermal characterization, whose adopted experimental setup are reported in Fig. 3a–c, respectively. Each test has specific goal in relation to the validation of the electrical characteristics of samples. In particular, the correlations between the stress–strain field and the electric output is investigated in view of sensing applications of conductive materials. The effect of heat treatments after the printing and their influence of the mentioned mechanical-electric response is also investigated. Finally, the ability to measure the dynamic response of one structure through the electric output of conductive materials is tested.

Tensile tests

The samples with integrated conductive wires are subjected to axial tensile force; the force and strain instant values are measured together with the instant values of the electric resistance of the conductive material. The goal of the tensile tests is to evaluate the behaviour of the conductive materials in the elastic field. Three samples were fabricated and tested per each conductive material (two variants) and wire width (three variants).

Printing parameter	Standard recommended	Fili (AIMPLAS)	Filaflex conductive (RECREUS)
Printing temperature [°C]	225	265	230
Flow rate [%]	100	120	110
Printing speed [mm/s]	25	10	6
Line width [mm]	0.4	0.3	0.3

Table 1. Result of the printing parameter optimization of the conductive filaments, in comparison with standard recommended values for the filler-free filament.

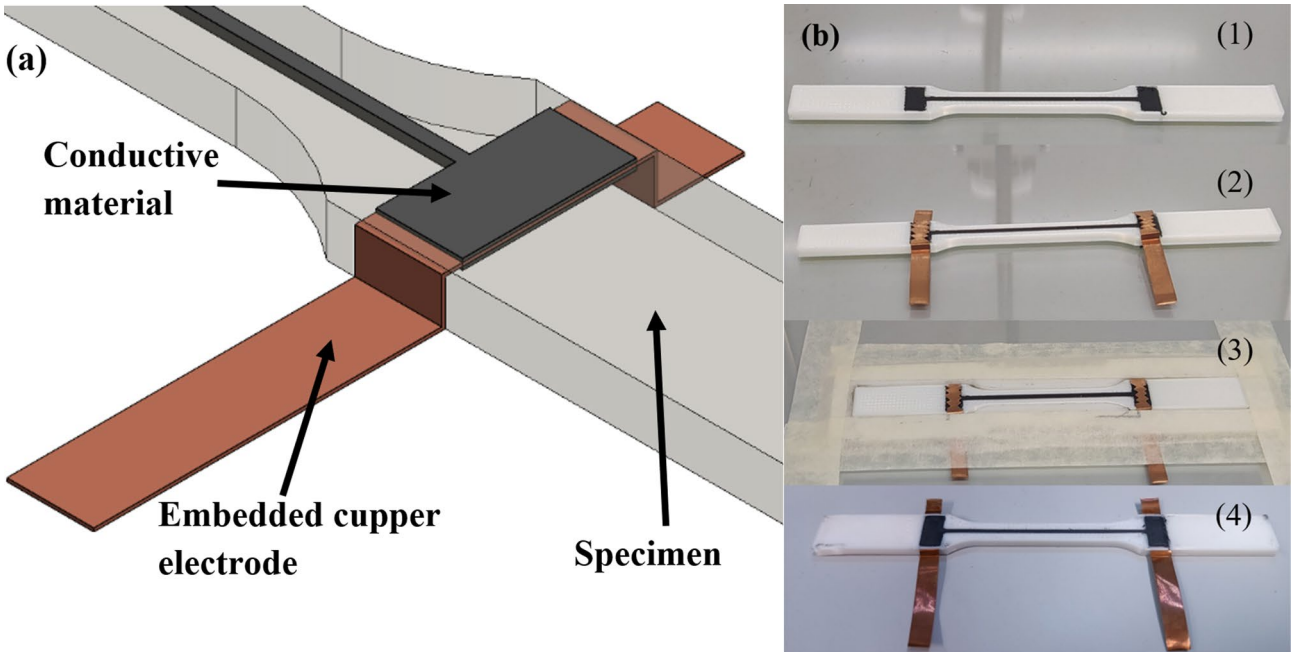

Fig. 2. Sample layer composition after the embedding of the conductive layer (**a**). Creation of the interface between the conductive material and copper electrodes (**b**): the printing process is interrupted at a certain layer (1), the copper plates are applied (2), securing of the electrodes with a jig and tapes (3), final shape of the sample, after the printing re-start, with copper plates embedded (4).

The tensile tests are performed with the INSTRON 8801 universal testing machine with displacement control mode at 1 mm/min velocity. The applied force varies in the range 0–400 N. The effective strain rate on the specimen is measured with an uniaxial dynamic extensometer (INSTRON 2620–604) referred to 22.5 mm gauge length. The testing machine is controlled with the software Bluehill. The acquisition of the data generated by the testing machine, the extensometer and the conductive material is provided with a 4-channels DAQ system (National Instruments CompactRIO-9054 and NI-9219 module). The experimental setup is reported in Fig. 3a.

The configuration of the DAQ system is developed in LabVIEW environment and allows the recording of the load, the strain returned by the extensometer and the electrical resistance of the conductive wire over the time domain, with 100 Hz sampling frequency. The post-processing of the recorded data is performed with MATLAB. The voltage divider is applied to the electrical resistance signal measured on the conductive wire, to respect the measurement range of the NI-9219 module. Prior the tensile test, the volume resistance of the specimen is recorded with a Fluke 114 multimeter and then the resistivity is estimated as:

$$\rho = R_0 \cdot \frac{\mathrm{A}}{L} \tag{1}$$

where ρ [Ω cm] is the electrical resistivity, R_0 [Ω] is the electrical resistance measured at the start of the test, A [cm^2] and L [cm] represent the cross-section and the length of the conductive track, respectively.

The results are presented graphically, and their suitability for application as strain gauges is evaluated using the gauge factor and the coefficient of determination. The gauge factor is defined as:

$$GF = \frac{\delta R/R_0}{\varepsilon} \tag{2}$$

where GF [dimensionless] is the gauge factor, ε [dimensionless] is the mechanical strain,δR [kΩ] represents the change in electrical resistance between the initial resistance and the resistance at a given ε. The coefficient of determination is defined as:

$$R^2 = 1 - \frac{\sum_{i=1}^{n} \left(Y_i - \hat{Y}_i\right)^2}{\sum_{i=1}^{n} \left(Y_i - \overline{Y}\right)^2} \tag{3}$$

where R^2 [dimensionless] is the coefficient of determination,Y_i [dimensionless] represents the i-th of n observed values of the analysed phenomenon,$\widehat{Y_i}$ [dimensionless] is the predicted value of the i-th observation provided by the estimation model, $\overline{Y}$ [dimensionless] is the mean of all observed values.

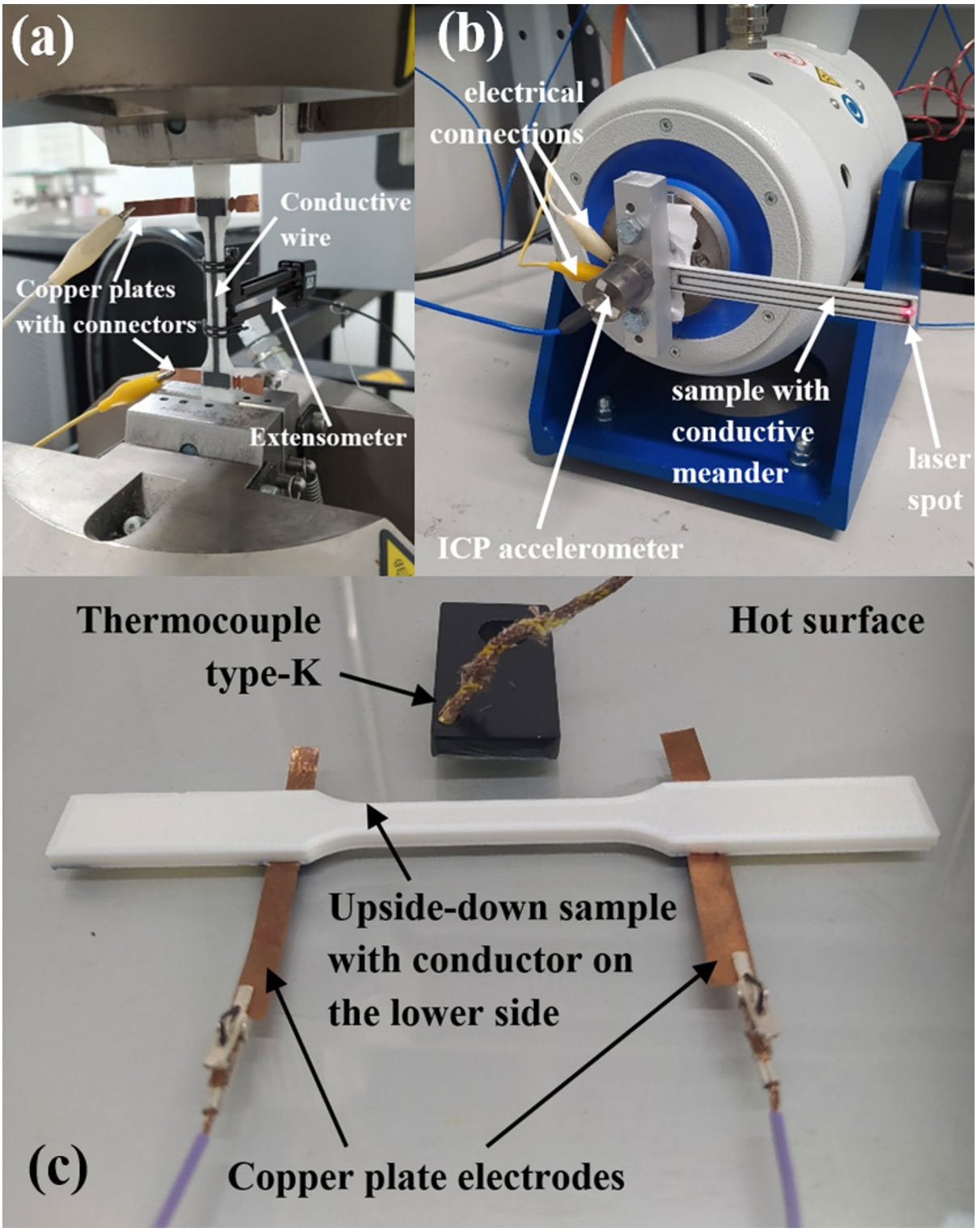

Fig. 3. Experimental setup: tensile test (**a**), dynamic test (**b**) and thermal test (**c**).

Thermal tests

The primary goal of the thermal tests is to determine if the value of electrical resistance of the embedded conductive wire is sensitive to the environmental temperature. Another goal is to identify eventual beneficial effects of heat treatments applied to the conductor, leading to an increase of the resistance-strain sensitivity for transducers applications. The tests consider the temperature variation on the component after the filament deposition, while the filament heating during the extrusion is considered as a constraint of the optimized process setup.

The sample with embedded conductive wire is heated by thermal conduction through direct contact with a hot surface for long time (five hours followed by one hour for cooling down). The instant electric resistance is measured at regular time intervals during the heating process, with sampling frequency of 100 Hz. The setup of the thermal tests is reported in Fig. 3c.

The values of electrical resistance and temperature are measure with the same DAQ system described before. The same voltage divider circuit is also used to measure the electrical resistance of the conductive wire. One sample per combination of conductive material (two variants) and wire width (three variants) was measured. A type-K thermocouple, calibrated with Fluke 123 equipped with the 80TK thermocouple module, is the sensor used to measure the instant temperature of the hot plate. The temperature range imposed to the hot plate is 0–140 °C, then the maximum temperature is kept constant for five hours. After this time, the heating system is turned off and one hour time is waited for the cooling down of the sample, by continuing the measurements.

Dynamic tests

In the dynamic tests, a beam sample with integrated conductive material is excited in the frequency domain and its vibrational response is measured. The vibration measurements obtained with a laser and with the conductive material used as a strain sensor are compared, with the goal to understand their agreement. The ultimate goal is to demonstrate the feasibility of dynamic measurements on FDM components, in terms of response amplitude and frequency, with an embedded sensor made of conductive material.

The experimental setup, represented in Fig. 3b, consists of a mechanical shaker (TV 51,120 TIRAvib) connected to a power amplifier (BAA 500 TIRAvib). The sample is a cantilever beam, with a conductive pattern on the top, connected to one end to the shaker. An ICP accelerometer (353B34 PCB) is fastened to the shaker stage to measure the excitation. The dynamic response of the free end of the sample is measured with a laser doppler vibrometer (VibroONE VIO130 Polytec).

The ADC/DAC (analog-to-digital / digital-to-analog controller) cRIO-9054 (National Instruments) is used to manage all the tests data. The sinusoidal signal used to actuate the shaker, through the amplifier, is generated with the NI-9263 module. The accelerometer output signal and the electric resistance of the conductive meander are measured with the NI-9234 module with a sampling frequency of 1652 Hz. This module is compatible with IEPE accelerometers, then no further instrumentation is needed. The same voltage divider circuit already described before is used to measure the conductor resistance.

The ADC/DAC is managed by a control interface self-developed in LabVIEW environment. The excitation is represented by a sequence of sinusoidal signals with a frequency increasing of a given step. The interface allows the user to set the frequency range and the step of frequency increment; the excitation voltage generated by the DAC is also imposed through the interface. When a new frequency is applied, the measurements starts with some time delay to wait the extinction of the transitory. The signals generated by the accelerometer (excitation), by the laser (tip response) and by the conductive meander are measured at each frequency and stored.

Before to start the sample characterization, the response is preliminary measured across a wide frequency range to identify the resonances, using DAC excitation voltages of 0.5, 1 and 1.5 V in the range 10–100 Hz, with step of 1 Hz. Then, the test is repeated on a narrower frequency range centred on the first resonance with step of 0.2 Hz and the same amplitudes.

The post-processing of the measured data is operated with MATLAB. The results are represented by means of two frequency response functions (FRFs), or gain functions, in the frequency domain, showing the structural response and the electro-mechanical response given by the conductive meander. The FRF of the beam structure is:

$$\left|G\left(f\right)_{struct}\right| = \frac{\ddot{Y}_{tip}}{\ddot{X}_{base}} \tag{4}$$

where.

$G(f)_{struct}$ [*adim*] is the FRF of the structure (i.e. cantilever beam), $\ddot{Y}_{tip}$ [m/s^2] is the acceleration amplitude of the system response measured at the free tip of the beam with the laser vibrometer, and $\ddot{X}_{base}$ [m/s^2] is the acceleration amplitude of the excitation measured on the shaker stage with the ICP accelerometer. The FRF of the electro-mechanical system composed by the beam with coupled conductive meander is:

$$\left|G\left(f\right)_{electro-mech}\right| = \frac{R\left(f\right)_{meander}}{\ddot{X}_{base}} \tag{5}$$

where.

$G(f)_{electro-mech}$ [kΩ/ m/s^2] is the FRF of the electro-mechanical system composed by the beam and the embedded conductive meander [kΩ/ m/s^2] and $R_{meander}$ [kΩ] is the electrical resistance amplitude at given frequency f.

Results

This Section reports the results of the experimental tensile, thermal and dynamic tests on the samples described before.

Tensile tests results

All tensile tests were performed at ambient temperature on samples produced directly through the FDM process, without any additional heat treatment. Three variants of conductive wires, with widths of 0.4 mm, 0.8 mm, and

	Initial electrical resistance (R_0) [kΩ]				Initial electrical resistivity (ρ_0) [Ω • cm]	
	Fili – AIMPLAS		Filaflex conductive—RECREUS		Fili—AIMPLAS	Filaflex conductive—RECREUS
Wire width [mm]	Mean value	St. Dev	Mean value	St. Dev	Mean value	Mean value
0.4	31.50	1.92	327.69	45.61	13.75	142.99
0.8	17.26	2.32	170.56	33.41	15.06	148.85
1.6	10.86	2.09	89.54	19.56	18.96	156.29

Table 2. Average values of the electrical resistances (R_0) and resistivity (ρ_0) over the applied strain range (0–0.012) for the two materials with different widths of the conductor.

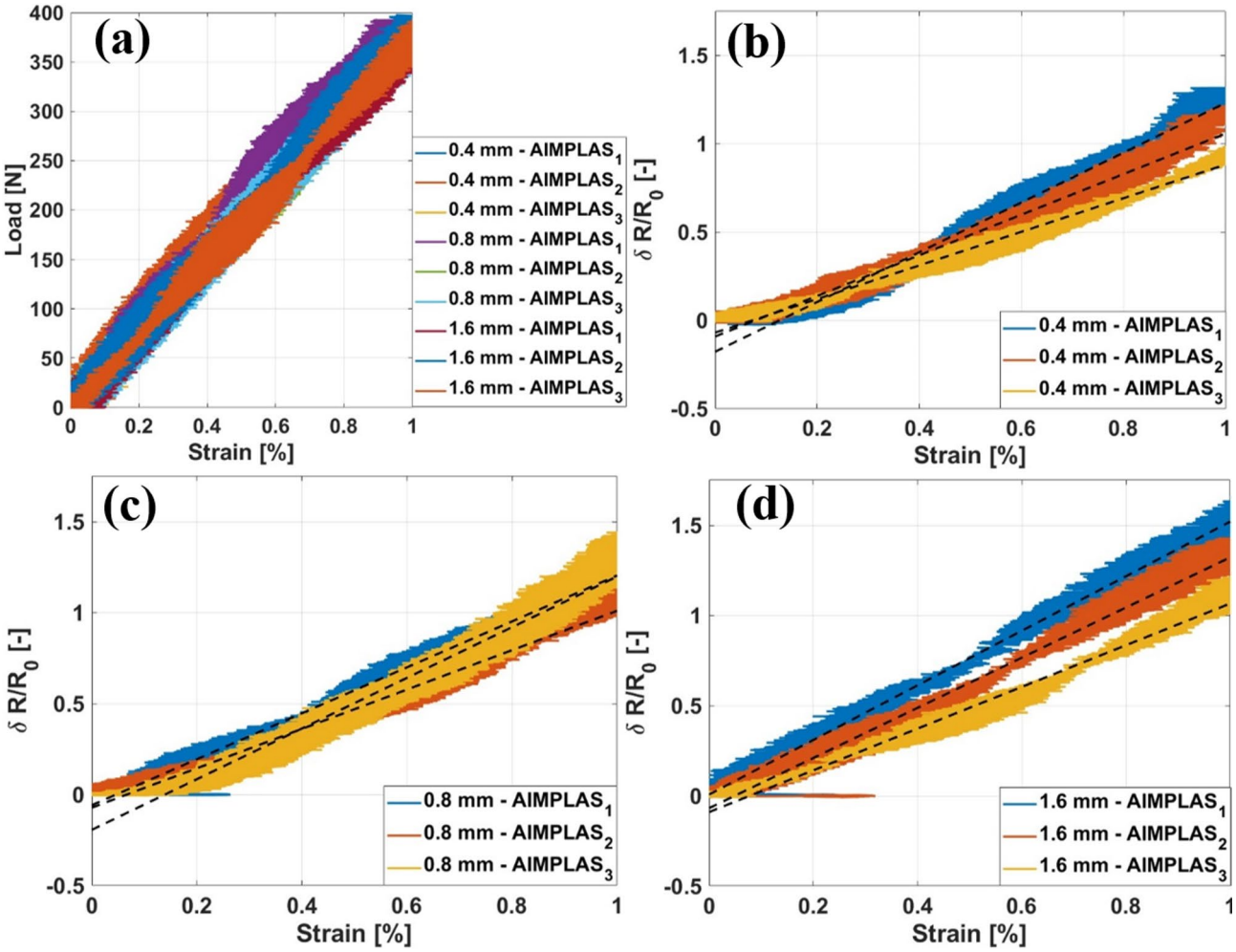

Fig. 4. Tensile test results on Fili – AIMPLAS material: load-strain curve (**a**), normalized electrical resistance variation ($\delta R/R_0$) under applied strain for conductive paths of varying widths: 0.4 mm (**b**), 0.8 mm (**c**), and 1.6 mm (**d**).

1.6 mm, were tested with the equipment previously described at 1 mm/min strain rate. Three samples have been tested for each wire width variant. Table 2 reports the values of electrical resistance and resistivity measured at variable applied strain.

The answer to the discrepancy with the supplier's data can be found in the model adopted to evaluate the resistivity reported in Eq. 1. This model doesn't consider additional conduction mechanisms such as electrical contact between adjacent nanoparticles or tunnelling effect[33].

The tensile test results for Fili—AIMPLAS and Filaflex Conductive—RECREUS materials are reported in Figs. 4 and 5, respectively. For both materials, the load-strain curves are shown in Figs. 4a and 5a, while the normalized electrical resistance variation ($\delta R/R_0$) under applied strain for different widths (0.4, 0.8, and 1.6 mm) is presented in Figs. 4b–d and 5b–d, respectively. The signals were acquired with a sampling frequency of 100 Hz. Over the tensile test, both the strain, the load and the resistance signals are affected by noise over the time

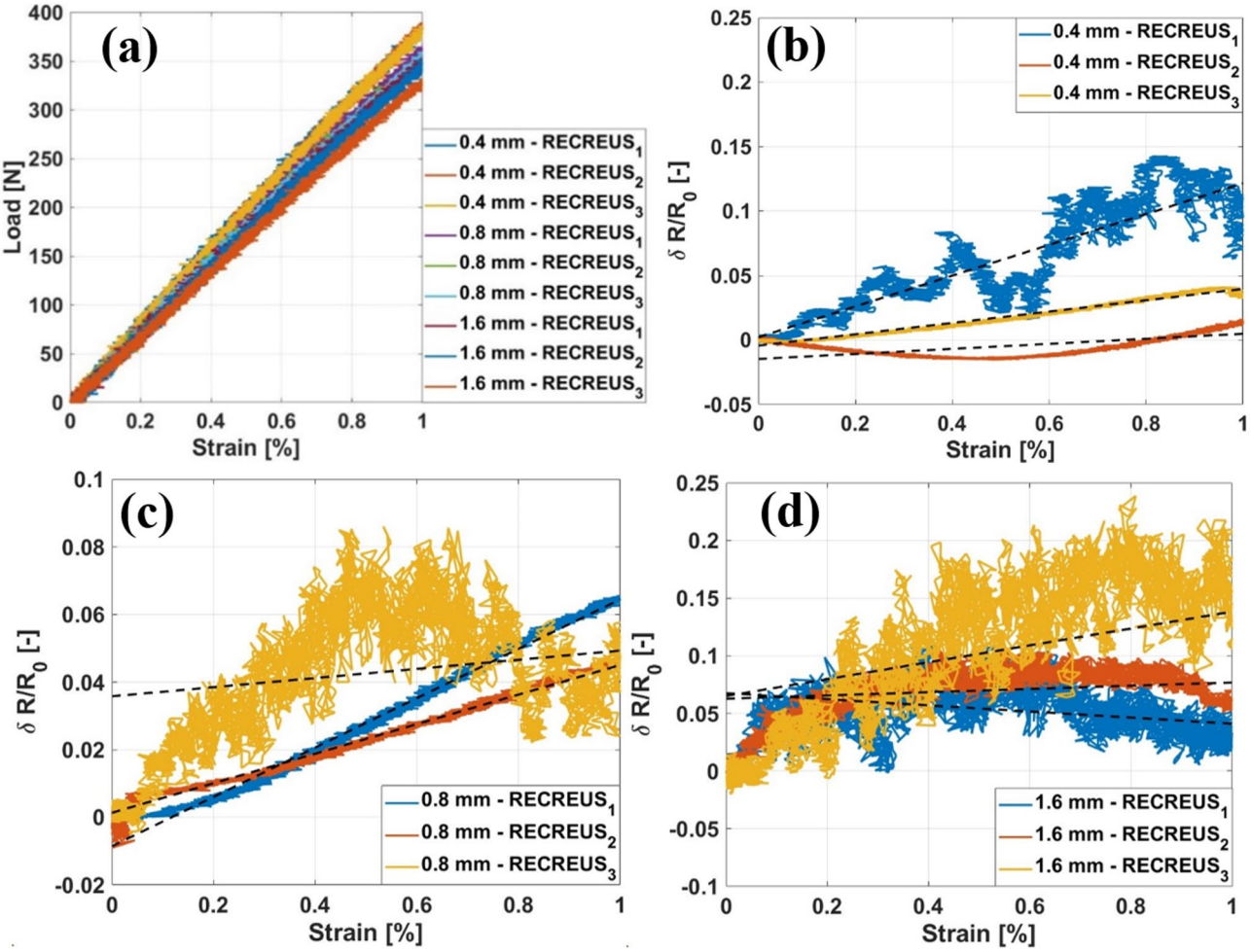

Fig. 5. Tensile test results on Filaflex Conductive—RECREUS material: load-strain curve (**a**), normalized electrical resistance variation ($\delta R/R_0$) under applied strain for conductive paths of varying widths: 0.4 mm (**b**), 0.8 mm (**c**), and 1.6 mm (**d**).

	Gauge factor (GF) [adim]				Coefficient of determination (R^2) [adim]			
	Fili—AIMPLAS		Filaflex conductive—RECREUS		Fili—AIMPLAS		Filaflex conductive—RECREUS	
Wire width [mm]	Mean value	St. Dev	Mean value	St. Dev	Mean value	St. Dev	Mean value	St. Dev
0.4	117.03	25.46	6.09	5.20	0.960	0.016	0.717	0.266
0.8	121.97	17.08	4.33	2.97	0.956	0.018	0.686	0.533
1.6	129.59	15.73	2.02	4.96	0.970	0.006	0.161	0.081

Table 3. Gauge Factor (GF) and Coefficient of Determination (R^2) for electrical resistance vs. applied strain in conductive wires of different widths.

domain. The reason why Figs. 4 and 5 for a certain resistance correspond multiple values for the strains is due to the fact that the variability introduced by the noise affecting the strain is larger than the variability exhibited by the resistance because the more the values of R_0 is larger, the more the effect of noise on the value of $\delta R/R_0$ is irrelevant.

Table 3 reports the gauge factor (GF) and the coefficient of determination (R^2) for the electrical resistance in wires with different widths. The range of the reported values for Fili–AIMPLAS and their low variability are in agreement with the literature[33]. On the other hand, in some samples of Filaflex Conductive—RECREUS, since the behaviour of the material is variable, the linear regression does not represent faithfully the measured response. This is testified by the values of the coefficient of determination (up to 0.717). The poor quality of the linear regression, together with low gauge factor suggests that the CB is not reliable when meant for strain sensing applications.

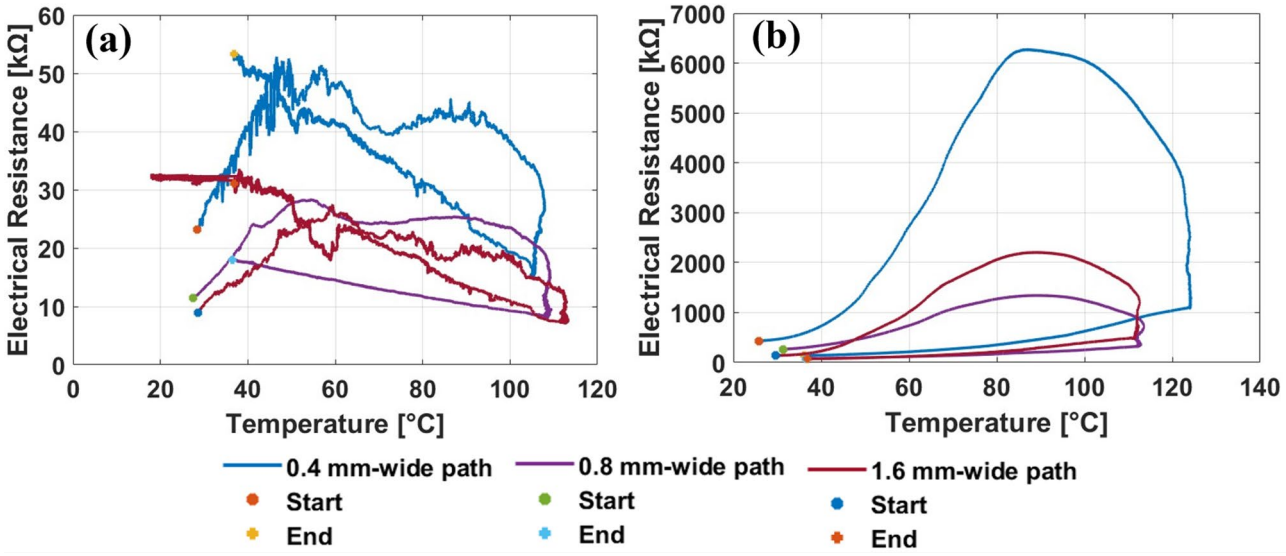

Fig. 6. Electrical resistance variation as function of the applied temperature for the Fili—AIMPLAS (**a**) and the Filaflex Conductive—RECREUS (**b**) materials with reference to different wire widths.

	Electrical resistance variation after heat treatment (kΩ)					
	Fili—AIMPLAS			Filaflex Conductive—RECREUS		
Wire width (mm)	Initial	Final	Variation	Initial	Final	Variation
0.4	23.14	53.26	+56.55%	430.25	135.60	−68.48%
0.8	11.47	36.42	+36.42%	264.82	77.82	−70.61%
1.6	8.9	31.65	+31.65%	138.46	72.02	−47.98%

Table 4. Electrical resistance variation after the heat treatment for the two materials with different widths of the conductor.

Thermal tests results

The thermal test is conducted by controlling the hot plate including heating, nominally from 20 to 140 °C, followed by constant temperature. The duration of these two steps is five hours. Finally, one hour for plate cooling down. The actual thermal profile returned by the thermocouple exhibits an average maximum temperature of 112° with high variability (standard deviation of 6.48 °C), due to the placing conditions of the thermocouple for each test. Anyway, the thermal profile is the same for all the specimens since the actual temperature is set by a different close-loop control thermocouple.

The results of electrical resistance variation during the thermal test (Fig. 6) highlight different behaviors. During the transition to the maximum temperature, the resistivity of both CPCs initially increases along with the temperature. According to the literature, this behavior is attributed to the difference in thermal expansion coefficients between the nanofiller and the polymer matrix[42].

The literature reports the existence of CPCs in which the electrical resistance follows the same trend as temperature during both heating and cooling, without hysteresis[31,42]. In our case, at the maximum temperature, the resistivity decreases in both CPCs. This behavior can be attributed to the fact that the maximum temperature reached in our study is 140 °C. At this elevated temperature, the polymer matrix can better accommodate the contact between conductive fillers. In contrast, studies where the maximum temperature remains below 60 °C do not observe such mechanisms[31,42].

However, major differences in the filler type is highlighted in the cooling stage. The use of 2D-fillers like graphene fillers in the Fili-AIMPLAS result in a rise in the resistance as the temperature decrease, and this can be due to the detrimental effect of temperature on the filler contact resistance[43]. At contrary, 0D fillers like CB particles in the Filaflex-RECREUS rearrange during the cooling process resulting in a resistance reduction. The way heat propagates through the component could influence the shape of the thermo-electric curve, potentially causing a delay in resistance changes.

Therefore, temperature induces permanent changes in the electrical properties of the CPCs. The permanent change in resistance observed in Fili-AIMPLAS and Filaflex-RECREUS, as reported in Table 4, is a typical behavior of CPCs. Commonly, the relationship that correlates the variation in resistance with temperature

change is referred to as the Negative Temperature Coefficient (NTC) and Positive Temperature Coefficient (PTC) effect, respectively[33,44].

A cyclic thermal treatment is performed to evaluate the progression of resistance variation observed in Fig. 6. The same samples already tested in Fig. 6 are used for evaluating the effects of thermal cycling. This choice is motivated by the needing to preserve exactly the same characteristics and features of the sample in terms of geometry, electrical interfaces and material. For the "Fili" filament, the same electrical resistance achieved at the end of the previous testing (about 50 kΩ) has been found at the beginning of the further thermal cycling. Similarly for the "Filaflex" filament (resistance of about 130 kΩ). Then, thermal profiles consisting of three repetitions of temperature variations up to 140 °C, as previously described, have been applied to the previous specimens having 0.4 mm wire width. The test results, reported in Fig. 7, indicate that repeated thermal cycling induces a progressive decrease in electrical resistance. However, the rate of decrease becomes less evident as the number of cycles increases.

Dynamic tests results

The FRF of the beam structure and of the electro-mechanical system of "Fili—AIMPLAS" and "Filaflex Conductive—RECREUS" materials are summarized in Fig. 8. The FRF is performed with an up-sweep with a step of 0.2 Hz, which whom the amplitude of the electrical excitation (AoE) used to drive the mechanical shaker varies among 0.5, 1 and 1.5 V. Two samples are used for the tests, with nominal length of 102.8 ± 0.05 mm where the meander of the conductive material described in Fig. 1c is deposited.

For the beam provided with the "Fili—AIMPLAS" meander, the structural FRF of the beam (Fig. 8a) reveals a resonance peak at 69.2 ± 0.2 Hz. The electro-mechanical FRF of the meander (Fig. 8c) maintain a constant trend until it also reveal a resonance peak 69.2 ± 0.2 Hz and then stabilize again on lower values. The correspondence of structural and electrical resonances confirms, also in the dynamic regime, the direct proportionality between strain (i.e. modal strain in this case) and electrical resistance. There is no evidence of shifting effects of the resonance induced by electrical nonlinearities or parasitic capacitances in the conductor.

For the "Filaflex Conductive – RECREUS" material, the structural FRF of the beam (Fig. 8b) presents a resonance peak at 65.8 ± 0.2 Hz. The electro-mechanical response curves (Fig. 8d) show the existence of a close peak to 65.8 Hz, however the material is not recommended for dynamic sensing applications given that the peak is not pronounced it could be attributed to signal noise. The reason of such low sensitivity to the vibration may be justified by the balance in the formation and dismission of connections between the CB particles or to a major damping of the vibrations in the TPU matrix.

By comparing the resonances of the two structures, the slight difference of about 3.4 Hz is due to the different stiffness of the two deposited meander, because the same nominal dimensions are used, and the base structure is built with the same material.

In conclusion, the "Fili—AIMPLAS" material shows a clear electro-mechanical response with resonance synchronized to that of the structure, suggesting its potential use as a dynamic sensor based on the indirect measurement of the material strain through the electrical resistance. On the contrary, the "Filaflex Conductive—RECREUS" material does not return a clear and sensitive FRF matching the structural dynamics, then it is scarcely usable as dynamic transducer according to these results. On the other hand, the use of this second material in dynamic applications seems recommendable when electrical stability and insensitivity to modal deformations is needed. According to the author's knowledge, no dynamic investigation regarding CPCs was found in literature, meaning that this kind of analysis has not been yet deeply explored. In this sense, the present work can contribute to the literature in this regard helping in the understanding of the possible behaviour that carbon-based CPC can exhibit and consequent applications.

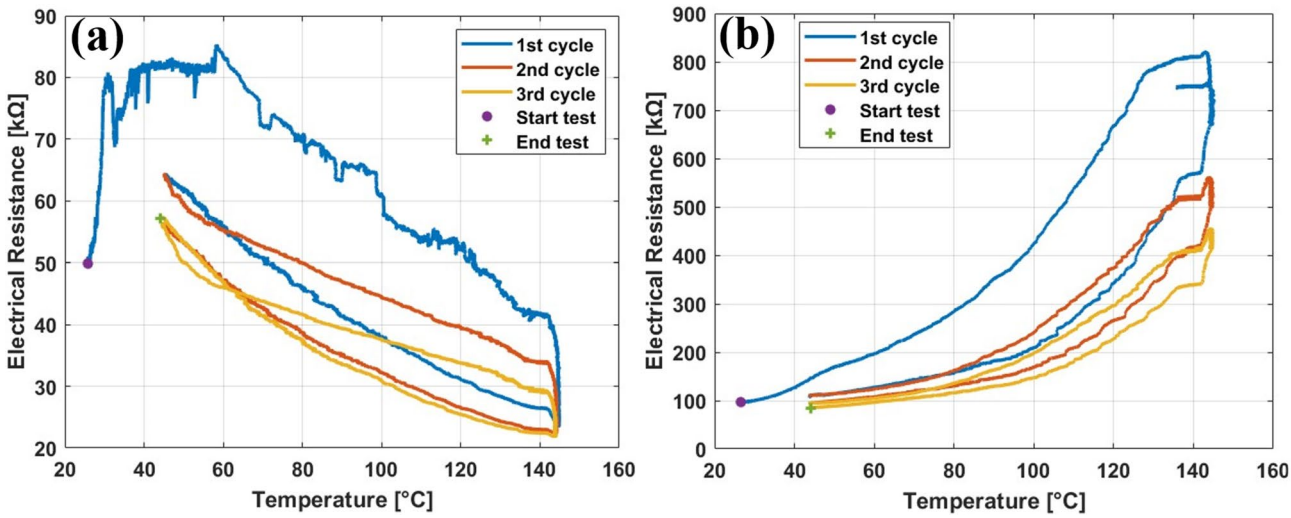

Fig. 7. Cyclical thermal treatment applied to Fili-AIMPLAS (**a**) and Filaflex-RECREUS (**b**).

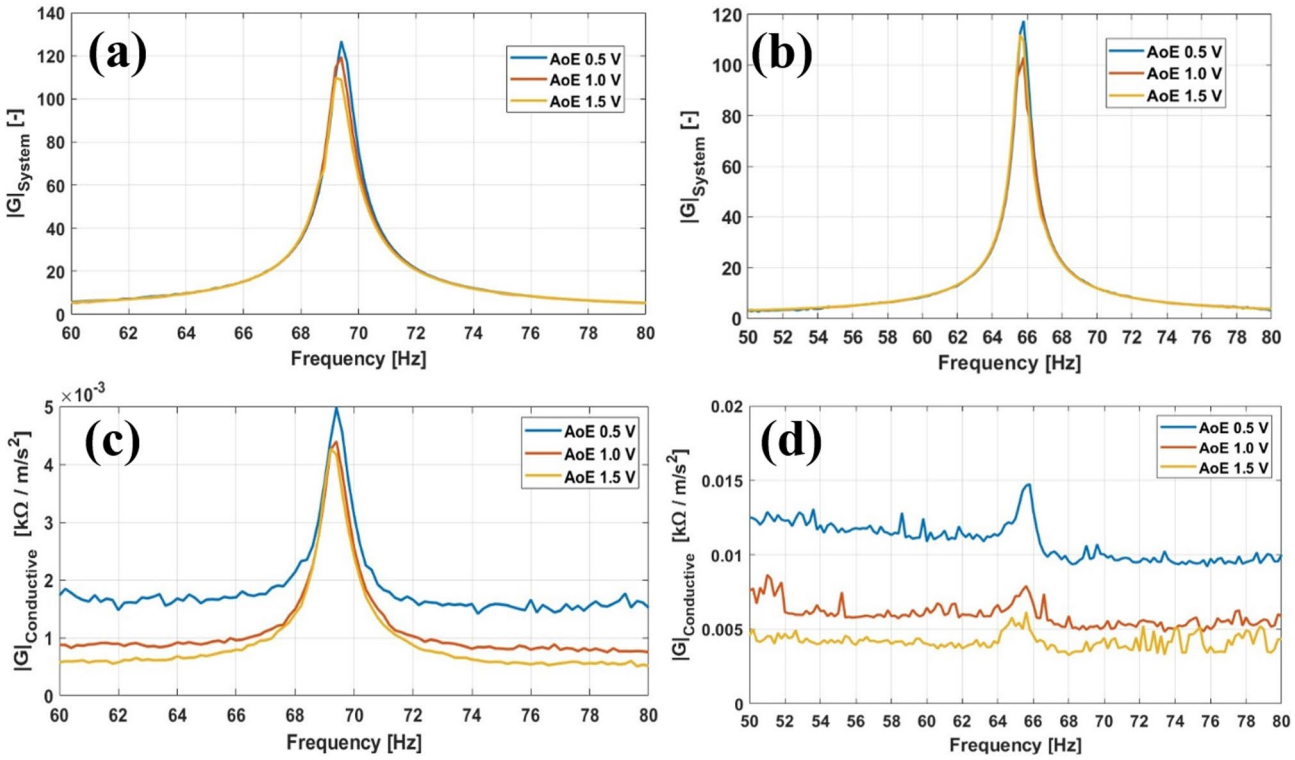

Fig. 8. Dynamic tests results of "Fili—AIMPLAS" : FRF of the beam structure (**a**) and FRF of the electro-mechanical (**b**), and FRF of the electro-mechanical system with frequency step of 1 Hz (**c**) and 0.2 Hz (**d**). The excitation amplitudes of 0.5, 1 and 1.5 V are reported for each curve.

SEM analysis

The scanning electron microscope (SEM) analysis on the two feedstock filaments is conducted with the aim to identify microstructural evidences of the observed static and dynamic electro-mechanical results. The back-scattered electrons (BSE) technique is also used to identify the presence of different phases into the material.

Scanning Electron Microscopy (SEM) analysis is one of the most extensively used scientific method employed when characterizing nano-particles[45]. In literature, other studies that investigated CPCs with SEM analysis assessed cryofracture surface[31,41]to assert the filler species of commercial filaments. The shape of the achieved cryofracture fractures depends on the fracture mechanics and may return pores shapes difficult to interpret. However, since these investigations only regard the cross-section of the filament, an investigation of the finished surfaces is proposed both in the axial and in the transversal direction to determine the magnitude of the pore presence in the filament feedstock.

The samples under investigation are represented by small segments of the filament feedstock, that must be analyzed preserving their original mechanical and physical properties. For this reason, the traditional process of sample encapsulation in polymer (e.g. bakelite) is not adequate due to the high temperatures involved.

The customized sample stub was manufactured from an aluminium rod with 20 mm cross-section diameter. The rod is milled to obtain the filament housing in transversal and axial directions for scanning tests. Epoxy adhesive is used to hold the filament segments into the housing.

Manual surface finishing is applied on the top side of the stub with P320, P600, P1200 and P2500 sandpaper and then Planar and Napal polishing cloths. After the finishing process, the stubs are dried in air for one day to reduce the content of water and the induced contaminations into the SEM vacuum chamber.

The SEM results of the "Fili—AIMPLAS" filament surfaces are reported in Fig. 9, and those ones for the "Filaflex Conductive—RECREUS" are reported in Fig. 10.

Discussions

In conclusion, the findings of the present study provides significant information about the properties of CPCs when processed with FFF, addressed to implementation in smart structures.

In the static tests, the mean initial resistance (R_0) of all tested specimens, measured at room temperature (Table 2), indicates that Filaflex Conductive-RECREUS exhibits an electrical resistance ten times higher than Fili-AIMPLAS, regardless of the conductive track width. Additionally, the recorded data confirm that an increased number of laid rasters reduces the overall resistance of the track. Moreover, the electrical resistivity measured experimentally deviates from the values provided by the suppliers. These findings align with the literature, as CPCs filled with graphene and CNTs, such as Fili-AIMPLAS, typically exhibit standard deviations below 3%, whereas CB-based CPCs, like Filaflex Conductive-RECREUS, tend to show greater variability in resistance[41].

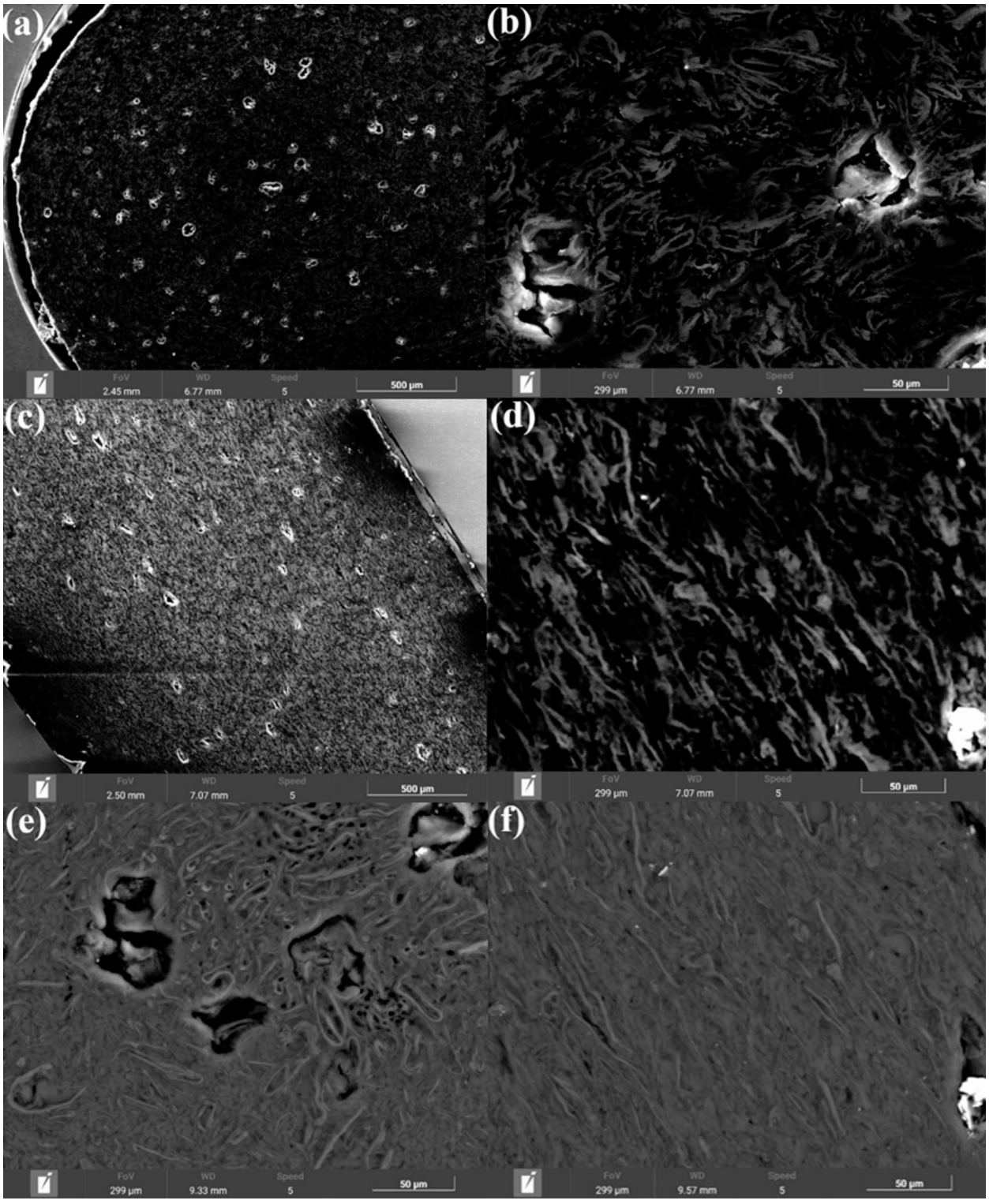

Fig. 9. SEM images of the "Fili—AIMPLAS" filament: transverse cross section (**a**, **b**), axial cross section (**c**, **d**), BSE transverse cross section (**e**), and BSE axial cross section (**f**).

From the static measurement of the force-strain gain factor (Figs. 4 and 5), there are not significant differences among the samples with variable geometry (in particular, 0.4, 0.8 and 1.6 mm width corresponding to 1, 2 and 4 extruded paths respectively). This confirms the insensitivity of the resistance variation with respect to the shape of the printed wire. Of course, when measuring the absolute values of resistance, there is direct proportionality between wire width and conductivity.

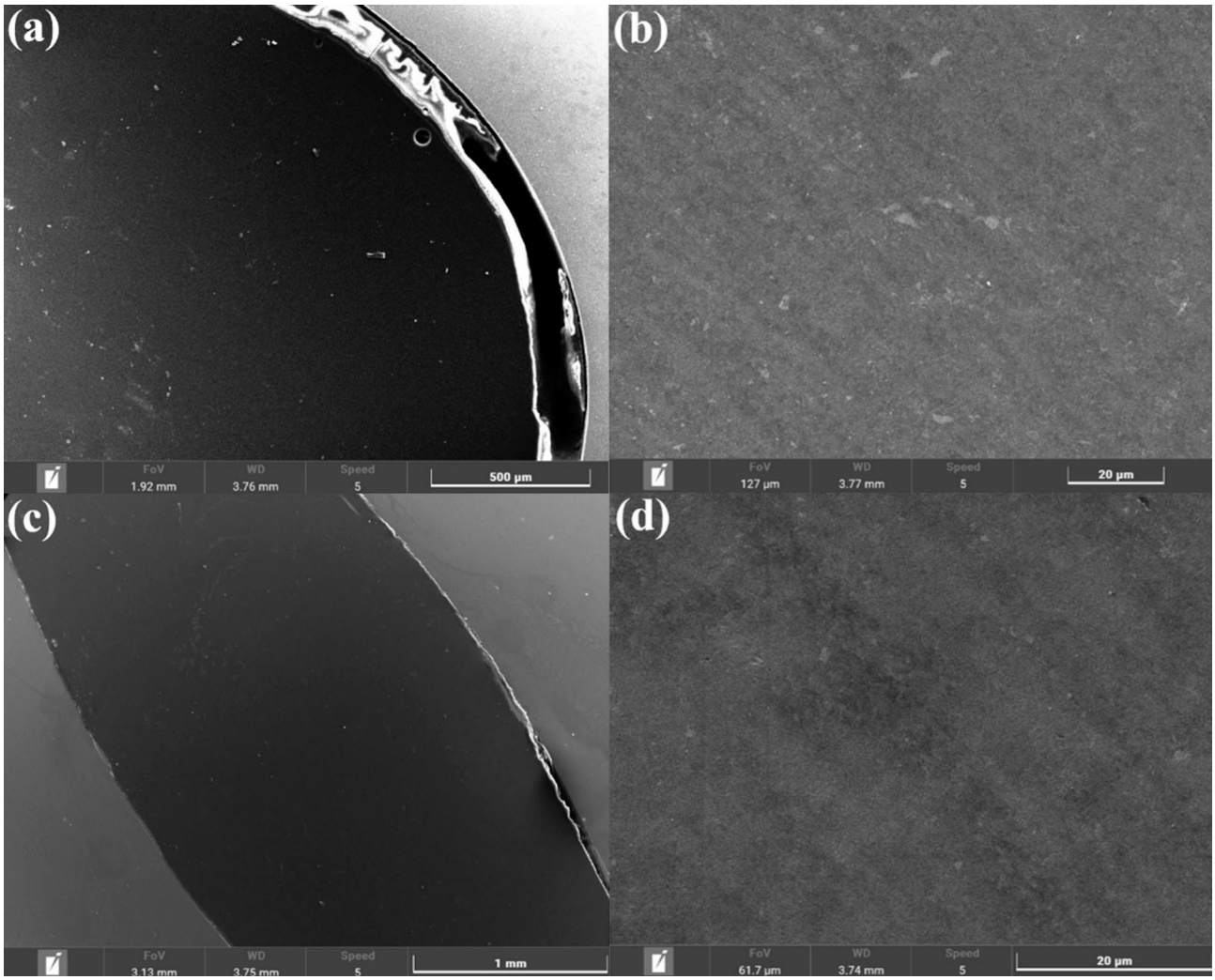

Fig. 10. SEM images of the "Filaflex Conductive—RECREUS" filament: transverse cross section (**a**, **b**), axial cross section (**c**, **d**).

The choice of filler type plays a crucial role in determining the material's behavior. As shown in Fig. 4, graphite-based CPCs, such as 'Fili-AIMPLAS,' exhibit a linear sensitivity to strain, demonstrating their suitability for strain sensing applications. Similarly, CB-based CPCs, such as 'Filaflex Conductive-RECREUS,' display a proportional response to strain, as evident from Fig. 5, although with lower linearity and higher signal noise. This difference is likely attributed to the contact between the particles of the so-called "0D filler"; this effect is not present in graphite fillers having lamellar shape.

In dynamic tests, a similar trend is observed: the CB-based filament is less sensitive to vibrations compared to the graphite-based filament. This behavior is likely due to the lower strain-resistance gains, which are difficult to detect with reasonable accuracy. Additionally, the modal shapes involved may induce simultaneous stretching and compression within the material, leading to a mutual compensation effect in electrical resistance variation.

Thermal tests revealed a significant impact of post-process heating on the overall resistivity. This effect can be attributed to changes in the properties of the nanofiller and local interactions between the filler and the polymer matrix. As the temperature increases, the electrical resistance of the material initially rises significantly (1.2 times for "Fili" filament and 13.6 times for "Filaflex" filament), followed by a sharp decrease, which can be explained by the thermal transition of the matrix's mechanical properties. Conversely, during cooling, the two analyzed materials exhibit different behaviors. The graphite-based CPC ("Fili") shows an increase in resistance (+ 237%), likely due to the permanent loss of internal conductive pathways. In contrast, the CB-based CPC exhibits a decrease in resistance of about -87% (Table 2), which can be associated with matrix shrinkage.

After multiple thermal cycles, the electro-thermal behavior of the CPCs is expected to stabilize along a characteristic curve. Indeed, 'Fili' exhibits nearly identical cooling curves in the second and third cycles, while the resistance variation over time decreases, as observed when comparing the heating curves of the first and third cycles. Similarly, 'Filaflex' shows a progressive reduction in maximum resistance with each cycle; however, no stabilization of its electro-thermal properties is observed. The application of severe thermal profiles exacerbates the resistance variation induced by temperature, though this phenomenon also occurs at lower temperatures.

In the literature, the validation of CPC-based temperature sensors is typically conducted using a single thermal test, often neglecting the gradual shift in electrical properties due to prolonged heat exposure. Thermal cycling tests confirm that these changes are both progressive and permanent. In conclusion, the results demonstrate that post-process heating generally leads to a loss of electrical conductivity. However, in some cases, heat treatments can partially restore the conductivity of the sensing material[31]. In both scenarios, the operating temperature of the filament after printing plays a crucial role in determining the material's electro-mechanical properties.

The SEM results showed that in the "Fili – AIMPLAS" filament, many pores are clearly visible into the filament before the melting process. Moreover, the BSE analysis confirms the presence of two different phases into the filament (Fig. 9e and f): a TPU/PLA matrix (dark color) and dispersed graphite filler in the shape of stripes (light color) or lamellas in 3-dimensions. By comparing the two section views, it seems that both voids and filler particles are deformed and stretched along the axial direction of the filament, that suggests a correlation of this shape with the feedstock extrusion production process. The presence of pores may be due to the shape of the graphene particles that could induce poor adhesion with the matrix during the production of the filament. The scanning images of the "Filaflex Conductive – RECREUS" filament show a continuous and homogeneous microstructure of the material with no significant voids inside. Also, there is no evidence of physical distinction between phases. The small spherical particles observed on the two cross sections are residuals of the polishing process. Both transverse and axial cross sections show the same surface texture. Globally, this second material shows high uniformity of its constituents.

The significant influence of the explored factors, along with the impact of additional variables such as humidity and acidity[33], suggests that the sensing device should be shielded from environmental exposure. To minimize the number of factors affecting the conductive properties of CPCs, embedding sensing devices within components is recommended[46]. The advantages of integrating CPCs into polymeric components manufactured via FFF are further supported by comparisons with competing processes, such as slurry casting and nano-coating, which are more complex, costly, and challenging to implement[8].

Conclusions

The experimental characterization and subsequent analysis of conductive filaments with nanoparticle fillers demonstrate the suitability of these materials for applications in sensing and smart structures. Key material properties and process-related effects have been investigated, providing deeper insights compared to most previous studies, which are often limited to basic material characterization. In particular, the influence of environmental factors, such as temperature, on the electro-mechanical properties of the conductors has been analyzed.

In general, research on CPCs is commonly conducted through the custom manufacturing of filaments. While this approach allows precise control over material parameters, it suffers from limited reproducibility, making it difficult to replicate results and thus constraining research advancements. Conversely, the use of commercial filaments overcomes some of the challenges related to the availability of specialized facilities required for custom filament production and enables the investigation of materials with consistent properties. However, the main limitation of commercial filaments lies in the incomplete knowledge of their exact composition and material properties.

Beyond the findings of this study, further research efforts are expected in the near future to achieve a comprehensive understanding of the electro-mechanical behavior of conductive filaments, their response to different loading conditions, and their linearity thresholds in real-world applications.

Data availability

Experimental results, numerical results and models are available upon request to the authors.

Received: 22 October 2024; Accepted: 8 July 2025
Published online: 24 July 2025

References

1. Rajan, K., Samykano, M., Kadirgama, K., Harun, W. S. W. & Rahman, M. M. Fused deposition modeling: Process, materials, parameters, properties, and applications. *Int. J. Adv. Manuf. Technol.* **120**(3), 1531–1570 (2022).
2. Rajesh, K. D., Ganesh, N., Reddy, S. Y., Mishra, H. & Naidu, T. M. Experimental research on the mechanical characteristics of fused deposition modelled ABS, PLA and PETG specimens printed in 3D. *Mater. Today Proc.* https://doi.org/10.1016/J.MATPR.2023.06.343 (2023).
3. Ngo, T. D., Kashani, A., Imbalzano, G., Nguyen, K. T. Q. & Hui, D. Additive manufacturing (3D printing): A review of materials, methods, applications and challenges. *Compos. B Eng.* **143**, 172–196 (2018).
4. Alami, A. H. et al. Additive manufacturing in the aerospace and automotive industries: Recent trends and role in achieving sustainable development goals. *Ain Shams Eng. J.* **14**, 102516 (2023).
5. Duan, L., D'hooge, D. R. & Cardon, L. Recent progress on flexible and stretchable piezoresistive strain sensors: From design to application. *Prog. Mater. Sci.* **114**, 100617 (2020).
6. Liu, H. et al. 3D printed flexible strain sensors: From printing to devices and signals. *Adv. Mater.* **33**, 2004782 (2021).
7. Joshi, A., Goh, J. K. & Goh, K. E. J. Polymer-based conductive composites for 3D and 4D printing of electrical circuits. *3D and 4D Printing of Polymer Nanocomposite Materials: Processes, Applications, and Challenges* 45–83 (2020) https://doi.org/10.1016/B978-0-12-816805-9.00003-X.
8. Park, S. & Fu, K. K. Polymer-based filament feedstock for additive manufacturing. *Compos. Sci. Technol.* **213**, 108876 (2021).
9. Ning, F., Cong, W., Qiu, J., Wei, J. & Wang, S. Additive manufacturing of carbon fiber reinforced thermoplastic composites using fused deposition modeling. *Compos. B Eng.* **80**, 369–378 (2015).
10. Galos, J., Hu, Y., Ravindran, A. R., Ladani, R. B. & Mouritz, A. P. Electrical properties of 3D printed continuous carbon fibre composites made using the FDM process. *Compos. Part A Appl. Sci. Manuf.* **151**, 106661 (2021).

11. Horst, D. J., de Andrade Junior, P. P., Duvoisin, C. A. & Vieira, R. D. Fabrication of conductive filaments for 3d-printing: Polymer nanocomposites. *Biointerface Res. Appl. Chem.* **10**, 6577–6586 (2020).
12. Zhou, X., Wu, L. & Wang, J. Recent developments in conductive polymer composites for fused deposition modeling. *Compos. Part A Appl. Sci. Manuf.* **174**, 107739 (2023).
13. Bunde, A. & Dieterich, W. Percolation in composites. *J. Electroceram.* **5**, 81–92 (2000).
14. Pejak Simunec, D. & Sola, A. Emerging research in conductive materials for fused filament fabrication: A critical review. *Adv. Eng. Mater.* **24**, 2101476 (2022).
15. Ren, H. et al. Smart structures with embedded flexible sensors fabricated by fused deposition modeling-based multimaterial 3D printing. *Int. J. Smart Nano Mater.* **2022**, 447–464 (2022).
16. Musenich, L. et al. Anisotropic mechanical and sensing properties of carbon black-polylactic acid nanocomposites produced by fused filament fabrication. *Smart Mater. Struct.* **33**, 095010 (2024).
17. Kouvatsos, T., Pagonis, D. N., Iakovidis, I. & Kaltsas, G. Towards a 3D printed strain sensor employing additive manufacturing technology for the marine industry. *Appl. Sci.* **14**, 6490 (2024).
18. Gackowski, B. M., Goh, G. D., Sharma, M. & Idapalapati, S. Additive manufacturing of nylon composites with embedded multi-material piezoresistive strain sensors for structural health monitoring. *Compos. Part B Eng.* https://doi.org/10.1016/j.compositesb.2023.110796 (2023).
19. Kwok, S. W. et al. Electrically conductive filament for 3D-printed circuits and sensors. *Appl Mater Today* **9**, 167–175 (2017).
20. Marasso, S. L. et al. PLA conductive filament for 3D printed smart sensing applications. *Rapid Prototyp J* **24**, 739–743 (2018).
21. Maurizi, M. et al. Dynamic measurements using FDM 3D-printed embedded strain sensors. *Sensors* https://doi.org/10.3390/s19122661 (2019).
22. Omar, M. H., Razak, K. A., Ab Wahab, M. N. & Hamzah, H. H. Recent progress of conductive 3D-printed electrodes based upon polymers/carbon nanomaterials using a fused deposition modelling (FDM) method as emerging electrochemical sensing devices. *RSC Adv* **11**, 16557–16571 (2021).
23. João, A. F. et al. 3D printing pen using conductive filaments to fabricate affordable electrochemical sensors for trace metal monitoring. *J. Electroanal. Chem.* **876**, 114701 (2020).
24. Hook, A., Motes, D. T., Morrow, C. & Donnell, K. M. Additively Manufactured Aperture-based FSS. *Conference Record–IEEE Instrumentation and Measurement Technology Conference* (2024) https://doi.org/10.1109/I2MTC60896.2024.10560971
25. Podsiadły, B., Skalski, A., Wałpuski, B. & Słoma, M. Heterophase materials for fused filament fabrication of structural electronics. *J. Mater. Sci.: Mater. Electron.* **30**, 1236–1245 (2019).
26. Jayanth, N., Senthil, P. & Mallikarjuna, B. Experimental investigation on the application of FDM 3D printed conductive ABS-CB composite in EMI shielding. *Radiat. Phys. Chem.* **198**, 110263 (2022).
27. Flowers, P. F., Reyes, C., Ye, S., Kim, M. J. & Wiley, B. J. 3D printing electronic components and circuits with conductive thermoplastic filament. *Addit. Manuf.* **18**, 156–163 (2017).
28. Hampel, B., Monshausen, S. & Schilling, M. Properties and applications of electrically conductive thermoplastics for additive manufacturing of sensors. *Tech. Mess.* **84**, 593–599 (2017).
29. Dembek, K., Podsiadły, B. & Słoma, M. Influence of process parameters on the resistivity of 3D printed electrically conductive structures. *Micromachines* **13**, 1203 (2022).
30. Palmić, T. B., Slavič, J. & Boltežar, M. Process parameters for FFF 3D-printed conductors for applications in sensors. *Sensors* **20**, 4542 (2020).
31. Stankevich, S. et al. Electrical resistivity of 3D-printed polymer elements. *Polymers* **15**, 2988 (2023).
32. Yu, G. et al. Thermoplastic elastomer composite filaments for strain sensing applications extruded with a fused deposition modelling 3D printer. *Flex. Printed Electron.* **5**, 035002 (2020).
33. del Bosque, A., Sánchez-Romate, X. F., Sánchez, M. & Ureña, A. Toward flexible piezoresistive strain sensors based on polymer nanocomposites: A review on fundamentals, performance, and applications. *Nanotechnology* **35**, 292003 (2024).
34. Aloqalaa, Z. Electrically conductive fused deposition modeling filaments: Current status and medical applications. *Crystals* **12**, 1055 (2022).
35. Coluccia, A. & De Pasquale, G. Strain-based method for fatigue failure prediction of additively manufactured lattice structures. *Sci. Rep.* **13**, 1–16 (2023).
36. De Pasquale, G. & Coluccia, A. Modeling and experimental validation of CFRP–metal joints utilizing 3D additively manufactured anchors. *J. Manuf. Sci. Eng.* **145**(11), 111004 (2023).
37. De Pasquale, G., Enes Altunok, F. & Ursi, F. Investigation of the mechanical strength of CFRP with co-cured additively manufactured metal inserts. *Proce. Struct. Integr.* **47**, 573–578 (2023).
38. De Pasquale, G. & Sibona, S. Hybrid materials based on polymers-filled AM steel lattices with energy absorption capabilities. *Mech. Adv. Mater. Struct.* **29**, 2570–2580 (2022).
39. De Pasquale, G. & Ursi, F. Multi-material fittings with carbon fiber reinforcement from AM process: design and characterization. In *3rd Int. Symp. on Industrial Engineering and Automation (ISIEA)* (Bolzano (Italy), 2024).
40. D638 standard test method for tensile properties of plastics. https://www.astm.org/standards/d638.
41. Nowka, M., Katja Ruge, L. S., Hilbig, K. & Thomas, V. Characterization of the anisotropic electrical properties of additively manufactured structures made from electrically conductive composites by material extrusion. *Polymers* https://doi.org/10.3390/polym16202891 (2024).
42. Alessandro Ragolia, M. *et al.* Thermal characterization of electrical resistance of 3D printed sensors. https://doi.org/10.1109/I2MTC50364.2021.9459968.
43. Fernández Sánchez-Romate, X. X., del Bosque, G. A., Sánchez, M. & Ureña, A. Electrical transport mechanisms in graphene nanoplatelet doped polydimethylsiloxane and application to ultrasensitive temperature sensors. *ACS Appl. Mater. Interfaces* **15**(18), 22377–22394 (2023).
44. Chu, K. et al. Smart conducting polymer composites having zero temperature coefficient of resistance. *Nanoscale* **7**, 471–478 (2014).
45. Solangi, N. H., Karri, R. R., Mubarak, N. M. & Mazari, S. A. Mechanism of polymer composite-based nanomaterial for biomedical applications. *Adv. Ind. Eng. Polym. Res.* **7**, 1–19 (2024).
46. Dhinesh, S. K. et al. Recent trends in additive manufacturing of electronics devices. *Mater. Today Proc.* **66**, 928–941 (2022).

Author contributions

Ferdinando Ursi: data acquisition, experimental tests, data interpretation, writing. Giorgio De Pasquale: conceptualization, design of the work, data interpretation, work financement, writing and revising.

Funding

This paper was funded by the Horizon Europe grant "HORIZON-CL4-2022-RESILIENCE-01", Project MIMOSA (Project 101091826).

Declarations

Competing interests

Authors declare they do not have any competing financial and/or non-financial interests in relation to this work.

Additional information

Correspondence and requests for materials should be addressed to G.P.

Reprints and permissions information is available at www.nature.com/reprints.

Publisher's note Springer Nature remains neutral with regard to jurisdictional claims in published maps and institutional affiliations.